Electronic structure of amorphous SiO_2: Experiment and numerical simulation

V. A. Gritsenko

Institute of the Physics of Semiconductors, Russian Academy of Sciences, Siberian Branch, 630090 Novosibirsk, Russia

R. M. Ivanov

Novosibirsk State University, 630090 Novosibirsk, Russia

Yu. N. Morokov

Institute of Computer Technology, Russian Academy of Sciences, Siberian Branch, 630090 Novosibirsk, Russia

(Submitted 13 June 1995)
Zh. Éksp. Teor. Fiz. **108**, 2216–2231 (December 1995)

The electronic structure of the amorphous oxide (a-SiO_2) on silicon is studied using x-ray emission and photoelectron spectroscopy. The experimental results are compared with the results of an MINDO/3 calculation of the cluster $((OH)_3–Si–O)_3–Si–O–Si–(O–Si–(OH)_3)_3$. It is found that near the top of the valence band the electronic states are determined not only by the nonbonding O $2p_\pi$ states, but also by the silicon atomic orbitals which interact with the oxygen $2p$ orbitals. The transport of electrons and holes in SiO_2 is analyzed from the standpoint of the results obtained. © *1995 American Institute of Physics.*

1. INTRODUCTION

Amorphous silicon dioxide (a-SiO_2) is a key element in silicon integrated circuits and optical glass fibers. The capture of electrons and holes in defects in the oxide results in a buildup of charge and, as a consequence, in degradation of the microcircuits. Optical transitions in defects cause distortion of the signals in a glass fiber. For these reasons, the electron spectra of a-SiO_2 and defects in it have been studied intensively.[1–6]

The investigation of the atomic density distribution function has provided evidence that fluctuations of the dihedral angle θ(Si–O–Si) in the 120–180° range with a maximum at 142–144° are observed in molten quartz and in the thermal oxide on silicon. The tetrahedral angle ψ(O–Si–O) is distributed in the 100–112° range with a maximum at 109°. The mean length of the Si–O bonds is 1.60 Å ± 10% (Refs. 2 and 7).

The purpose of the present work is to experimentally investigate the electronic structure of the thermal oxide on silicon using x-ray spectroscopy and to compare the experimental results with the results of the simulation of the electron spectrum of a-SiO_2 by the MINDO/3 method.

2. EXPERIMENTAL METHOD

Layers of a thermal oxide with a thickness of 1.2 μm, which was obtained by oxidizing silicon in humid oxygen at 1050°C, were investigated. The x-ray photoelectron spectra of the O $1s$ and Si $2p$ atomic levels and the valence band were investigated on an HP5960A spectrometer. The spectra were excited by monochromatized radiation in the aluminum $K_{\alpha 1,2}$ line with an energy of 1486.6 eV. Calibration with respect to the energy was performed relative to the carbon $1s$ line with an energy of 285.0 eV or the gold Fermi level with an energy of 5.0 eV.

Information on the partial density of states in the valence band was obtained from x-ray emission spectra. This method is based on the creation of unoccupied states in atomic levels (Si $1s$, Si $2p$, and O $1s$) in the oxide by irradiation. These states are filled by electrons from the valence band. A valence band–atomic level transition is accompanied by the emission of x radiation. The intensity of the radiation is proportional to the density of electronic states in the valence band and the transition probability. Since the width of the valence band in a-SiO_2 is about 13 eV, it is generally assumed that the transition matrix element is weakly dependent on the energy. In this case the x-ray emission spectra reflect the distribution of the partial density of states in the valence band.

X-ray transitions in which the total orbital angular moment changes by unity ($\Delta l = \pm 1$) are allowed in the dipole approximation. For example, the Si $L_{2,3}$ x-ray emission spectra exhibit transitions from the Si $3s$, $4s$, and $3d$ states to the valence band at the silicon $2p_{1/2,3/2}$ level (the latter is designated as $L_{2,3}$ in spectroscopy). Thus, the Si $L_{2,3}$ x-ray emission spectrum reflects the distribution of the silicon $3s$, $4s$, and $3d$ states. The Si K spectra contain transitions from the Si $3p$ states to the Si $1s$ level. The Si K x-ray emission spectra reflect the distribution of the Si $3p$ states. The O K emission spectra are observed when an electron passes from an oxygen $2p$ level to the $1s$ level. These spectra contain information on the distribution of the O $2p$ partial density of states in the valence band.

The partial density of states in the conduction band is investigated using x-ray absorption spectra or quantum-efficiency spectra (QES). The absorption spectra contain transitions from deep atomic levels to unfilled states in the conduction band. The measurement of the absorption spectra of the oxide on silicon presents some specific technical difficulties. For this reason, the quantum-efficiency spectra, in

 1063-7761/95/121208-09$10.00

which Auger electrons are recorded, were investigated in the present work. Quantum-efficiency spectra reflect the partial density of states in the conduction band with accuracy to the dependence of the transition matrix element on the energy. Quantum-efficiency spectra obey the dipole selection rules.

The Si $L_{2,3}$ and O K x-ray emission spectra were investigated on a spectrometer–monochromator with a spherical diffraction grating. These spectra were excited by an electron beam. The beam current was ≈ 1 mA. The Si $L_{2,3}$ and O K quantum-efficiency spectra were excited by the bremsstrahlung of a W anode. The Si K quantum-efficiency spectra were excited by the bremsstrahlung of a Ta anode. The energy resolution as a function of the portion of the spectrum studied is:

in the case of quantum-efficiency spectra
for Si K—no poorer than 0.5 eV,
for Si $L_{2,3}$—0.2 eV,
for O K—0.8 eV;
in the case of x-ray emission spectra
for Si $L_{2,3}$—0.4 eV,
for O K—0.4 eV.

The experimental techniques were described in greater detail in Ref. 8.

The x-ray emission and quantum-efficiency spectra were juxtaposed on a single energy scale, in which the energy of an electron in a vacuum was taken as the zero reference point. The energies of the Si $2p$ and O $1s$ levels, which were determined by x-ray photoelectron spectroscopy (XPS), were used for this purpose. The energy of the Si $1s$ level was determined from Si K_α spectra, in which transitions between the Si $2p$ and Si $1s$ levels are recorded. The energy of this transition measured in the oxide was equal to 1740.5 eV. The procedure for juxtaposing the spectra was described in Ref. 2.

3. ELECTRONIC STRUCTURE OF a-SiO_2 ACCORDING TO X-RAY SPECTROSCOPIC DATA

The x-ray emission (Si $L_{2,3}$, O K), quantum-efficiency (Si $L_{2,3}$, Si K, O K), and x-ray photoelectron spectrum of the conduction band of the thermal oxide on silicon which we measured are presented in Fig. 1. The Si K x-ray emission spectra for quartz were taken from Ref. 9, and the ultraviolet photoelectron spectrum of a thin (56 Å) dry oxide on silicon was taken from Ref. 10. Here and in the following the spectra are juxtaposed on a single energy scale, on which the energy of an electron in a vacuum was taken as the zero reference point. The experimental spectra were normalized in relative units separately for the valence band and the conduction band to the maximum values of the peaks in these bands. The dotted lines in Fig. 1 depict our calculated partial densities of states, which were normalized to a single maximum value over the entire range of energies. Scaling factors equal to 4 and 6 were introduced into the calculated curves in the case of the Si $3p$ partial density of states in the valence band and the O $2p$ partial density of states in the conduction band, respectively, for a more graphic comparison with the experimental curves. The positions of the band edges E_c and E_v are indicated in Fig. 1 by vertical dashed lines.

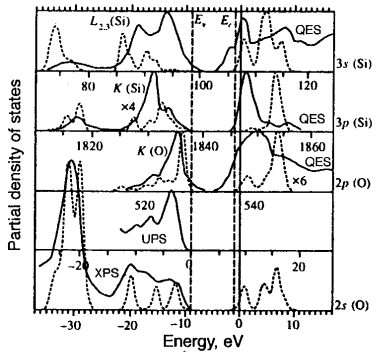

FIG. 1. Experimental emission and quantum-efficiency spectra of the thermal oxide on silicon. The Si K emission spectra were taken from Ref. 9, and the ultraviolet photoelectron spectrum (UPS) of thin SiO_2 (56 Å) was taken from Ref. 10. The dotted lines are the calculated partial densities of states for the $Si_8O_{25}H_{18}$ cluster.

According to core photoemission data, the electron affinity of the thermal oxide on silicon is equal to 1.0 eV (Ref. 2). This means that the bottom of the conduction band E_c of a-SiO_2 is 1.0 eV below the vacuum level of an electron. According to optical absorption and photoconductivity data, the band gap of the thermal oxide on silicon at room temperature has a width equal to 8.0 ± 0.1 eV (Ref. 11). Thus, the top of the valence band E_v is 9.0 eV below the level of an electron in a vacuum. Such a value of E_v corresponds to the height of the potential barrier for holes on the Si–SiO_2 boundary $\phi_n=3.8$ eV. This value coincides with the value obtained in experiments on the photoemission of holes in the Si–SiO_2 system[12] and in experiments on the ultraviolet photoelectron spectroscopy of the Si–SiO_2 boundary $\phi_n=3.95\pm0.08$ eV (Ref. 13).

A comparison of the x-ray spectra of the thermal oxide on silicon with the spectra of quartz oxide and crystalline α-quartz from Ref. 9 reveals that the positions and shapes of the density-of-states peaks in these three materials do not differ. These data indicate that the main features of the electronic structure are determined by the short-range order in the arrangement of the atoms. The absence of translational symmetry does not cause significant changes in the spectrum of the electronic states in the valence band and in the conduction band.

The complete valence band of a-SiO_2 consists of two valence bands. The lower narrow band is formed from O $2s$ states with an admixture of Si $3s$ and $3p$ states. The width of the upper valence band amounts to about 13 eV. It follows from Fig. 1 that there are high-energy tails extending into the band gap in the Si $L_{2,3}$ and O K x-ray emission spectra. The nature of these tails has not yet been elucidated. It can be speculated that they are caused by many-electron effects.

The low-energy tail in the O K quantum-efficiency spectrum also extends into the band gap. The low-energy peak in the Si $L_{2,3}$ quantum-efficiency spectrum is located in the band gap. These phenomena cannot be explained in the one-electron theory. It has been theorized that the low-energy

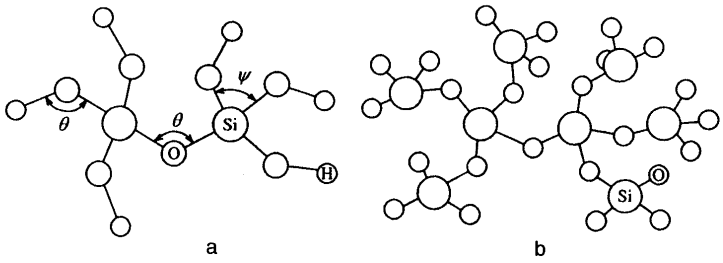

FIG. 2. Structure of the $Si_2O_7H_6$ (a) and $Si_8O_{25}H_{18}$ (b) clusters. The H atoms are bonded to surface O atoms. The H atoms are not shown in part b.

peak in the Si $L_{2,3}$ quantum-efficiency spectrum is caused by an x-ray exciton.[14]

4. MODEL AND CALCULATION METHOD

The calculations of the electronic structure of SiO_2 were performed in the cluster approximation using the quantum-chemical MINDO/3 method.[15] The parametrization for calculating SiO_2 was taken from Ref. 5. The parameters in Ref.5 were selected by reproducing the properties of molecules containing Si–O bonds.

The achievement of self-consistency in the MINDO/3 method is especially important when the electronic structure of local defects in SiO_2 is considered. In this case the geometric relaxation of the atoms near each defect must be taken into account. In calculating the energies of localized states, the relaxation of the electronic structure following the filling of these states is important and requires the achievement of self-consistency.

The parametrization of the MINDO/3 method from Ref. 5 has several shortcomings, one of which is the underestimation of the degree of charge transfer to the Si–O bond. The experimental data in Ref. 16 attest to the fact that the degree of charge transfer in this bond amounts to $0.5e$. Similar values are provided by the nonempirical calculations in Refs. 17–19. At the same time, the MINDO/3 method gives an appreciably smaller value of $0.3e$ for the degree of charge transfer. Another shortcoming, which was mentioned in Ref. 5, is the inaccurate description of the equilibrium Si–O–Si dihedral angle in the structure of silicon dioxide. The model gives an equilibrium angle equal to 180°, while the angle in α-quartz is 144°. The MNDO method, which is another widely used semiempirical method, also gives an equilibrium angle equal to 180°. Edwards and Fowler[5] attribute this result to the fact that the total energy varies only slightly, by hundredths of an electron volt, as the dihedral angle is varied from 180° to 140°. This means that we should rely on the experimental values of the dihedral angles to reproduce the electronic structure of α-SiO_2 in calculations.

We performed MINDO/3 calculations of the electronic structure of silicon dioxide on two clusters. Both clusters are centered on an oxygen atom. The smaller $(OH)_3$–Si–O–Si–$(OH)_3$ cluster (Fig. 2a), which is the same as the cluster in Refs. 5 and 6, contains only two silicon atoms. The larger $((OH)_3$–Si–$O)_3$–Si–O–Si–(O–Si–$(OH)_3)_3$ cluster (Fig. 2b) has two additional coordination spheres, which contain 6 silicon atoms and 18 oxygen atoms. As in Refs. 5 and 6, the dangling bonds of the outer oxygen atoms in both clusters are saturated by hydrogen atoms.

The $Si_2O_7H_6$ cluster (Fig. 2a) with a central atom surrounded by one coordination sphere was used to simulate the electronic structure of an oxygen vacancy in SiO_2 in Refs. 5, 6, 20, and 21.

Figure 3 compares our calculated partial densities of states in the smaller (dotted lines) and larger (solid lines) clusters. Unless stated otherwise, the calculated curves shown in this figure and the ensuing figures below, correspond to the values $\psi = 109°$, $\theta = 144°$, and L(Si–O) = 1.63 Å. It is seen that details of the electronic structure for these two clusters differ quite appreciably. For this reason, all the calculations, including the results presented in Fig. 1, were subsequently performed on the larger cluster.

Our calculations showed that in some cases the transition from the smaller cluster to the larger cluster can also result in profound changes in the relaxed atomic structure near the center of the cluster. In particular, when a positively charged oxygen vacancy was calculated, we took a starting geometry similar to the one used in Refs. 5 and 6. Optimization of the positions of the two central silicon atoms in the larger cluster led to a symmetric geometric structure for the defect and symmetric spatial localization of the unpaired electron on both atoms. In the smaller cluster similar relaxation gave an asymmetric geometric structure and asymmetric localization of the unpaired electron, which were previously obtained in Refs. 5 and 6.

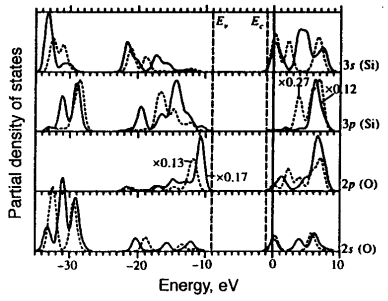

FIG. 3. Partial density of states for the smaller $Si_2O_7H_6$ cluster (dotted lines) and for the larger $Si_8O_{25}H_{18}$ cluster (solid lines). In this and the following figures the partial density of states was calculated for the central O atom and an Si atom bonded to it.

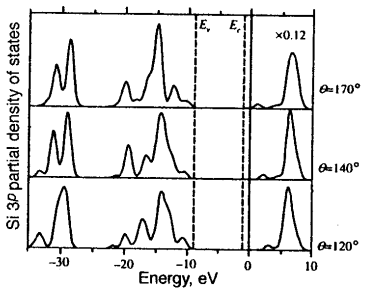

FIG. 4. Si $3p$ partial density of states for various values of the dihedral angle.

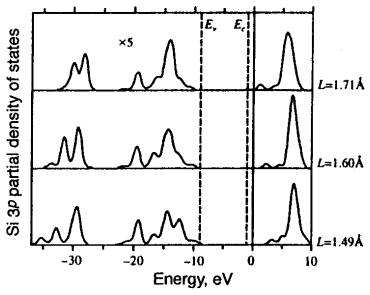

FIG. 6. Si $3p$ partial density of states as a function of the Si–O bond length.

5. INFLUENCE OF DISORDERING ON THE ELECTRON SPECTRUM OF SiO_2

To theoretically study the influence of disordering of the atomic structure, we varied the bond lengths in the cluster, as well as the values of the dihedral and tetrahedral angles. The results of the calculations are presented in Figs. 4–9.

The dihedral angle was varied simultaneously in all the Si–O–Si and Si–O–H fragments in the cluster. An increase in the dihedral angle from 120° to 170° is accompanied by displacement of the low-energy edge of the unfilled Si $3p$ states by ≈ 3 eV toward smaller energies (Fig. 4). At the same time, the position of the high-energy edge of the filled states remains unchanged.

The variation of the dihedral angle is accompanied by transformation of the distribution of the Si $3s$ states in the valence band. At all angles the Si $3s$ density of states is small near the top of the valence band (Fig. 5). In a first approximation the energy gap between the occupied and unoccupied states does not depend on the value of the dihedral angle. The gap for the Si $3s$ states is displaced toward more negative energies as the dihedral angle is increased.

The distributions of the oxygen $2p$ and $2s$ states in the valence band and the conduction band are weakly dependent on the value of the dihedral angle.

Increasing the Si–O bond length from $L=1.49$ Å to $L=1.71$ Å results in appreciable compression of the entire electronic structure, which is associated with a decrease in the overlapping of the atomic orbitals. Displacement of the unfilled and filled Si $3p$ states toward more negative energies is also observed (Fig. 6). This effect is not attributed to the electrostatic influence of the cluster boundary. Variation of the charge on the surface atoms of the cluster can cause displacement of all the states along the energy scale. However, evidence against such an explanation is provided by the displacement of the states forming the lower valence band (the range from -28 to -38 eV) toward positive energies. An increase in the Si–O length has a similar influence on the Si $3s$ partial density of states (Fig. 7). An increase in the length of the Si–O bond also results in displacement of the filled and unfilled O $2p$ states toward more negative energies (Fig. 8).

The displacement of the electronic states on the Si and O atoms as the Si–O distance is varied is not associated with charge transfer in the Si–O bond. This is evidenced by the simultaneous displacement of the O $2p$ and Si $3s$ states toward more negative energies.

The dependence of the degree of charge transfer Δq in the Si–O bond on the Si–O bond length and the dihedral angle θ was investigated. Variation of the bond length in the 1.57–1.63 Å range results in variation of the charges on the atoms by no more than 1.5%. An increase in θ from 120° to 170° is accompanied by nonmonotonic variations of Δq amounting to no more than 6%. Our findings correlate with the data in Ref. 3, which indicate that the degree of charge

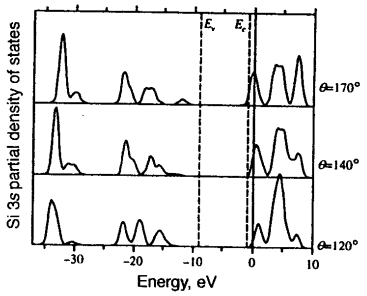

FIG. 5. Si $3s$ partial density of states for various values of the dihedral angle.

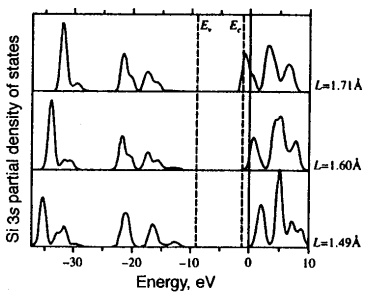

FIG. 7. Si $3s$ partial density of states as a function of the Si–O bond length.

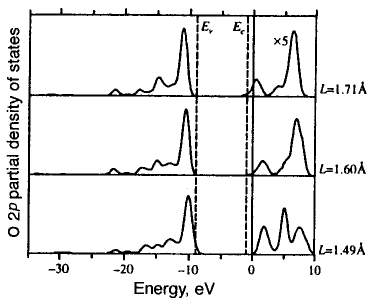

FIG. 8. O $2p$ partial density of states as a function of the Si–O bond length.

transfer does not depend on the magnitude of the dihedral angle. We note that these data are not consistent with the results in Refs. 17 and 18, in which it was found that the degree of charge transfer increases significantly as the dihedral angle is increased.

In addition to the fluctuations of the Si–O–Si dihedral angle and the Si–O bond length in a-SiO_2, the value of the O–Si–O tetrahedral angle (ψ) can also vary in the general case. In an ideal tetrahedron this angle has a value of 109.48°. According to Ref. 22 the mean fluctuations of the tetrahedral angle in SiO_2 do not exceed $\pm 0.7°$. However, according to the data in Ref. 7 the mean standard deviation of the tetrahedral angle in the amorphous oxide has a large value equal to $\pm 7°$. A value for the standard deviation of $\sim 2°$ was obtained in Ref. 23.

An increase in some O–Si–O tetrahedral angles is accompanied by a decrease in other tetrahedral angles. To obtain a picture of the influence of fluctuations of the tetrahedral angle on the electron spectrum of SiO_2, we varied the values of ψ in the following manner. The value of ψ for one of the Si–O bonds was established with respect to the other three Si–O bonds. Thus, the tetrahedral angles at all the silicon atoms were varied simultaneously.

Figure 9 presents the dependence of the Si $3p$ partial density of states on the value of ψ. An increase in ψ from 100° to 120° results in monotonic displacement of the filled and unfilled states toward more negative values by ~ 4 eV.

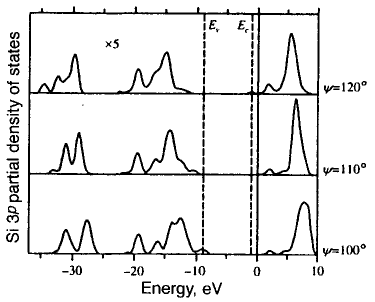

FIG. 9. Si $3p$ partial density of states as a function of the tetrahedral angle.

6. COMPARISON OF THE EXPERIMENTAL AND CALCULATED RESULTS

To simulate the electron spectrum of amorphous SiO_2, the partial density of states calculated for different values of the dihedral angles and Si–O bond lengths were summed with the experimentally determined distribution functions of these parameters for the thermal oxide on silicon.[7] The results obtained are presented in Fig. 1 and are discussed below.

Numerous band calculations of various modifications of crystalline SiO_2, particularly quartz, give the following results.[4,17,18,24] The upper broad valence band consists of three subbands. The lower subband is formed by the O $2p$, Si $3s$, and Si $3p$ orbitals. The upper narrow subband consists of the nonbonding O $2p_\pi$ orbitals which are oriented perpendicularly to the Si–O–Si plane. The middle subband is separated from the lower subband and consists of weakly bonding orbitals. These orbitals are formed mainly by the O $2p$ orbitals which lie in the Si–O–Si plane and are oriented perpendicularly to the Si–Si direction. Owing to the deviation of the Si–O–Si angle from 180°, these O $2p$ orbitals weakly overlap the Si $3s$ and $3p$ atomic orbitals.

The narrow band of O $2p_\pi$ orbitals corresponds to a large value of the hole effective mass $m_h^* = 5m_e - 10m_e$ (Ref. 24). According to Ref. 25, the narrow band of nonbonding O $2p_\pi$ orbitals near the top of the valence band and the large hole effective mass correspond to the low mobility of holes in SiO_2. Stefano and Eastman[25] attribute the low hole mobility to weak overlapping of the O $2p_\pi$ orbitals. Mott[26] attributes the low mobility of holes in SiO_2 to the formation of polarons localized on oxygen atoms. Both of these explanations for the low hole mobility are based on the idea that the states near the top of the SiO_2 valence band are determined by the nonbonding O $2p_\pi$ orbitals. Theories based on the localization of holes in the O $2p_\pi$ orbitals in a-SiO_2 are widely used to account for the buildup of positive charge in metal–oxide–semiconductor structures.

The distribution of the O $2p$ states is given by two different experiments. The ratio between the photoionization cross sections of the Si $3s$, Si $3p$, and O $2p$ states is such that the O $2p$ states predominate in the ultraviolet photoemission spectra at $\hbar\omega = 40.8$ eV. The O K emission spectra reflect the distribution of these states with accuracy to the dependence of the matrix element on the energy. The experimental results do not make it possible to separate the contributions of the nonbonding and bonding oxygen $2p_\pi$ states. However, in contrast to Refs. 4, 17, 18, and 24, the experimental results and our calculations point to the absence of a gap between the nonbonding and bonding oxygen states. We note that experimentally there is no such gap not only in a-SiO_2, but also in α-quartz.[9] The experimental results and the calculations agree on the point that the O $2p$ density of states decreases from the top to the bottom of the valence band. The calculated peak of the O $2p$ partial density of states is significantly narrower than the experimentally observed peak. The maximum is shifted toward the band gap. The calculation also predicts an underestimated density of states in the lower half of the valence band, which corresponds to bonding states.

The calculated peaks of the Si $3p$ density of states are shifted toward the top of the valence band in comparison to experiment. The calculation predicts a peak in the lower part of the valence band, which is not expressed experimentally. It is significant that the Si $3p$ states and, therefore, the O $2p$ states associated with them stretch up to the top of the valence band. This means that in the upper part of the valence band there are not only nonbonding O $2p_\pi$ states, but also weakly bonding O $2p$, Si $3s$, and Si $3p$ states. Their contribution to the total density of states amounts to about 1%.

The Si $L_{2,3}$ emission spectra reflect the transitions from the Si $3s$ and Si $3d$ states to the Si $2p$ level. The experimental Si $L_{2,3}$ spectrum has two peaks and a shoulder near the middle of the valence band (Fig. 1). The calculated form of the Si $3s$ partial density of states agrees poorly with experiment. The calculation predicts an insignificant, but finite Si $3s$ density of states near the top of the valence band. We note that all the known calculations of SiO_2 (Refs. 4, 18, 24, and 27) give an underestimated (in comparison with experiment) Si $3s$ density of states near the top of the valence band. It can be postulated that the large amplitude of the upper peak in the Si $L_{2,3}$ spectra is caused by a contribution of Si $4s$ and $3d$ states. The calculations performed in Refs. 24 and 28 do not support a contribution of Si $3d$ states to the SiO_2 valence band. However, the calculations in Ref. 29 indicate that the high-energy peak in the Si $L_{2,3}$ spectra is, in fact, caused by Si $3d$ orbitals.[29] Calculations of Si_3N_4, whose structural unit is an SiN_4 tetrahedron, also support the contribution of Si $3d$ orbitals near the top of the valence band.[30]

Thus, the experimental Si $L_{2,3}$ and Si K emission spectra, as well as the x-ray photoelectron spectra of the valence band, indicate that the states near the top of the valence band are determined not just by the nonbonding O $2p_\pi$ orbitals. Contributions to the density of states near the top of the valence band E_v are also made by silicon $3s$ and $3p$ states and possibly by $3d$ and $4s$ states. These atomic states form weakly bonding orbitals with oxygen $2p$ states. The calculation also predicts a contribution of O $2s$ states over the entire valence band (Fig. 1).

In band-structure terms the top of the a-SiO_2 valence band is doubly degenerate. There are heavy holes with $m_h^* = 5m_e - 10m_e$, which correspond to the O $2p_\pi$ orbitals. There should also be light holes corresponding to weakly bonding orbitals.

The band models of heavy and light holes in a-SiO_2 are not rigorously applicable due to the absence of long-range order. However, as will be seen below, the models of heavy and light holes in a-SiO_2 are confirmed experimentally. According to experiment, the fraction of $3s$ and $3p$ states in the lower valence band amounts to about 20% of the fraction of the states in the upper valence band (Fig. 1). The calculated value is approximately four to five times greater than the experimentally observed value. Similar results were obtained in Refs. 3, 4, and 27. This disparity can be attributed to the dependence of the x-ray transition matrix element on the energy. Such an hypothesis means that the probability of the transition of electrons which genetically belong to $3s$, $3d$ and $3p$ levels from the upper valence band to the Si $2p$ and Si $1s$ levels is significantly greater than the transition probability from levels corresponding to the lower valence band. This phenomenon can be caused, say, by the dependence of the form of the outer silicon atomic orbitals on the energy of the states formed with their participation. In our calculations, as well as in many others, the form of these orbitals remains fixed.

The calculated partial densities of states in the conduction band presented in Fig. 1 poorly reflect both the positions of the peaks in the quantum-efficiency spectra and their relative amplitudes. On the one hand, this is attributable to the limited size of the basis of valence states used. On the other hand, a more correct comparison of the calculated data obtained for the conduction band requires consideration of the electronic relaxation of the conduction band states when they are filled by electrons. It results in lowering of the energy of each such state by an amount of the order of the Coulomb repulsion energy between electrons found in the respective orbital. Due to the small linear dimensions of our clusters, this shift can be of the order of 1–2 eV. The calculation predicts a small Si $3p$ density of states near the bottom of the conduction band.

The experimental results provide evidence that the bottom of the a-SiO_2 conduction band is formed by Si $3s(3d)$, Si $3p$, and O $2p$ orbitals. Our calculations point out contributions of Si $3s$, O $2s$, and O $2p$ states. A contribution of Si $4s$ states to the formation of the bottom of the conduction band was noted in Ref. 19. Band calculations of α-quartz predict a small value for the electron effective mass $m_e^* = 0.3m_e$ (Ref. 24).

The calculations of the electronic structure of SiO_2 which we performed in the cluster approximation by the semiempirical quantum-chemical MINDO/3 method generally reproduce the main features of the electronic structure of the valence band, viz., the position of the top of the valence band, the width of the valence band, the position of the gap between the upper and lower valence bands, etc. At the same time, the approximations used do not promise a correct description of finer details of the electronic structure, viz., the exact positions and amplitudes of the individual partial density-of-states peaks. The plots in Fig. 3 demonstrate, for example, the marked influence of the cluster approximation on details of the electronic structure. Since the electronic structure of the SiO_2 valence band is determined by the short-range order, we assume that a further increase in the size of the cluster will not cause considerable variation of the partial density of states. Although the model used does not make it possible to accurately describe the details of the SiO_2 electronic structure, it seems useful for discussing and analyzing the experimental results obtained.

7. ELECTRON AND HOLE TRANSPORT IN SiO_2

The processes of electron transport in quartz glass and in the thermal oxide on silicon have been thoroughly studied. The concentration of intrinsic and impurity carriers in SiO_2 is negligibly small. The conductivity of quartz glass is mediated by nonequilibrium carriers, which are produced by generating electron–hole pairs. Their generation is generally

a result of irradiation by x rays or electrons. The conductivity of a-SiO_2 on silicon is mediated by nonequilibrium carriers injected from silicon (or the metal).

The value of the mobility for electrons $\mu_e = 20 \pm 3$ $cm^2/V \cdot s$ at 300 K was determined for quartz glass in fields $\sim 10^4 - 10^6$ V/cm in Ref. 31. A similar value $\mu_e = 29$ $cm^2/V \cdot s$ was obtained from Hall measurements for the thermal oxide and $F \sim 10^6$ v/cm (Ref. 32). The mobility $\mu_e = 20$ $cm^2/V \cdot s$ corresponds to $m_e^* \simeq 1.4 m_e$. The drift velocity of electrons in SiO_2 is saturated at $V \sim 10^7$ cm/s. This value corresponds to the equality $mV^2/2 \sim \hbar\omega_{LO}$ (here $\hbar\omega_{LO}$ is the energy of the longitudinal-optical phonons).[33]

The momentum electron mean free path $l_p = 34$ Å was determined in experiments involving the photoinjection of electrons into the thermal oxide on silicon in fields equal to $10^5 - 10^6$ V/cm (Ref. 34). A similar value $l_p = 32$ Å was obtained when hot electrons were injected from a depleted silicon layer on a Si–SiO_2 boundary.[35] Reimann and Onnasch[36] showed that the momentum mean free path increases from 31 Å at 12 K to 38.5 Å at 300 K. Thus, an electron mobility $\mu_e = 20$ $cm^2/V \cdot s$ corresponds to a mean free path $l_p \sim 30$–40 Å.

In relatively weak fields $F \sim 3 \times 10^6$ V/cm the dominant mechanism for scattering the energy and momentum of electrons is scattering on longitudinal-optical phonons.[37–39] The distribution function is strongly anisotropic, and forward scattering at small angles predominates.

The interaction of electrons with longitudinal-optical phonons is described by a Fröhlich electron–phonon interaction constant of the form

$$\alpha = \frac{q^2}{\varepsilon_p}\left(\frac{m^*}{2\hbar\omega_{LO}}\right)^{1/2}, \quad \varepsilon_p^{-1} = \varepsilon_\infty^{-1} = \varepsilon^{-1}. \tag{1}$$

Here ε_p, ε_∞, and ε are the polaron, optical, and low-frequency dielectric constants. In a-SiO_2 the longitudinal-optical phonons have characteristic energies equal to 0.153 eV and 0.063 eV. The values of the optical dielectric constant in a-SiO_2 are $\varepsilon_\infty = n^2 = 2.13$ (n is the refractive index), $\varepsilon = 3.96$, and $\varepsilon_p = 4.54$. For $m^* \simeq m_e$ we obtain $\alpha \simeq 2.1$.

The value of the electron–phonon interaction constant in SiO_2 is such that both the tight- and weak-binding approximations are poorly satisfied. In the weak-binding approximation ($\alpha \ll 1$) the polaron energy for $\hbar\omega_L = 0.153$ eV in SiO_2 is $W_p = \alpha\hbar\omega_L \simeq 0.32$ eV. The polaron mass is $m_p = (1 + \alpha/\sigma)m^* = 1.35m^*$. In the tight-binding approximation ($\alpha \gg 1$) the polaron energy is $W_p = 0.1\alpha^2\hbar\omega_p \sim 0.03$ eV. When an electron moves in a polaron lattice, such as the SiO_2 lattice, it puts on a "phonon coat." Its energy decreases by an amount equal to W_p. The mobility depends on the temperature according to a Boltzmann law:

$$\mu \propto \exp(-W_p/kT). \tag{2}$$

The experimental results indicate that in the 100–200 K range the mobility $\mu_e = 40$ $cm^2/V \cdot s$ does not depend on the temperature.[31] In the 200–300 K range the mobility decreases with the temperature.[31] According to the Thornber–Feynman theory,[37,31]

$$\mu \propto \frac{1}{\alpha m_e}\frac{e}{\hbar\omega_{LO}}\frac{3kT}{2\hbar\omega_{LO}}\exp\left(\frac{\hbar\omega_{LO}}{kT}\right). \tag{3}$$

This result indicates that in weak fields the mobility of electrons in a-SiO_2 is determined by the generation of longitudinal-optical phonons, rather than by localization due to the polaron effect. In strong fields $F > 3 \times 10^6$ V/cm scattering on acoustic phonons predominates. The distribution function then becomes significantly more isotropic. The energy electron mean free path equals 30–40 Å (Ref. 39). The value of the effective mass used to simulate electron transport in the conduction band in strong fields lies in the range from $0.5m_e$ to $1.4m_e$ (Ref. 39).

The value of the effective mass in the oxide on silicon is determined from the results of tunneling experiments on a semiconductor(metal)–oxide boundary in metal–oxide–semiconductor structures. The dependence of the current on the field F has the form

$$j = \frac{e^3F^2m_e}{8\pi\hbar\Phi m^*}\exp\left(-4\frac{(2m^*)^{1/2}\Phi^{3/2}}{3\hbar eF}\right). \tag{4}$$

Here Φ is the height of the barrier (in eV) at the metal(semiconductor)–SiO_2 boundary. Expression (4) corresponds to the simplest model of tunneling through a triangular barrier. The values $m_e^* = 0.4m_e$–$1.0m_e$ were obtained for the tunneling of an electron in SiO_2 in this approximation.[40–42] Experiments on the photostimulated tunneling of electrons at the Al–SiO_2 boundary gave the value $m_e^* = 0.5m_e$ in Ref. 43. The analysis performed in Ref.44 showed that the value of the effective mass increases by approximately 20% when the dispersion of the energy as a function of the momentum is taken into account according to the Franz law. Experiments on the tunneling of electrons in a thin oxide under conditions under which interference between the incident and reflected electron waves is observed[45–47] gave $m_e^* = 0.42m_e$–$0.85m_e$. Thus, depending on the model used for interpretation, the value of the tunneling effective mass of electrons moving across a barrier in the region of the SiO_2 band gap lies in the range from $0.4m_e$ to $0.9m_e$, which is close to the effective mass of electrons moving in the conduction band.

The value of the tunneling effective mass of light holes was determined in experiments involving the injection of holes at the Si–SiO_2 boundary. In Ref. 41 the injection of holes was investigated when an insulator was charged in a plasma. The value $m_h^* = 0.93m_e$ was obtained. Efimov, Meerson, and Evtukh[48] investigated the buildup of holes in a Si–SiO_2–Si_3N_4–Al structure. The value $m_h^* = 1.16m_e$ was obtained for $\Phi_h = 3.8$ eV. Similar experiments were performed in Ref. 49 on an Si–SiO_2–Ta_2O_5–Al structure. The value $m_h^* = 1.26m_e$ was obtained. The value $m_h^* = 0.5m_e$ was obtained in Ref. 50 for the tunneling of holes through a thin oxide (22.5 Å).

We note that in amorphous silicon nitride (a-Si_3N_4) the value of the tunneling mass for holes is small: $m_h^* = 0.3m_e$ (Ref. 51). In a-Si_3N_4 the valence band is also composed of nonbonding N $2p_\pi$ and bonding Si $3s$, Si $3p$, and N $2p$ orbitals.[52]

The value of the effective mass of the heavy holes in a-SiO_2 was determined in Ref. 53 by analyzing the temperature dependence of the fundamental absorption edge. The spectral dependence of the absorption edge α in SiO_2 is described by Urbach's empirical rule

$$\alpha=\alpha_0 \exp\left[-\frac{(\hbar\omega-E_g)\sigma}{kT}\right]. \quad (5)$$

Here α_0 and σ are parameters of the material, and E_g is the width of the band gap. In materials with an excitonic type of absorption, the broadening of the excitonic absorption is caused by longitudinal-optical phonons, according to Toyozawa's model. The theory relates the parameters of Urbach's rule to the reduced mass of an exciton $m_r^{-1}=m_e^{-1}+m_h^{-1}$.

$$\left(\frac{\sigma}{kT}\right)^{-1}=18\pi\left(\frac{1}{\varepsilon_\infty}-\frac{1}{\varepsilon}\right)\left(\frac{m_e}{m_r}\varepsilon_\infty a_0\right)^3\frac{\hbar\omega_{LO}}{2V_0}\tanh\left(\frac{\hbar\omega_{LO}}{kT}\right). \quad (6)$$

Here a_0 is the Bohr radius, and V_0 is the unit cell volume (113.09 Å^3 for a-SiO_2).

The analysis of the temperature dependence of the absorption edge of quartz glass in the 113-768 K temperature range gave the values $E_g=8.7\pm0.05$ eV, $\hbar\omega_{LO}=0.058$ eV, $m_r=0.3m_e$–$0.5m_e$, and $m_h\sim5m_e$ (Ref. 53). The value $\hbar\omega_{LO}=0.058$ eV is close to the value of 0.063 eV for the energy of a long-wavelength optical phonon. The small value of the exciton reduced mass in a-SiO_2 attests to the presence of heavy holes in SiO_2. The temperature dependence of the a-SiO_2 absorption edge experimentally confirms the existence of heavy holes corresponding to the narrow band of nonbonding O $2p_\pi$ orbitals.

Thus, the exponential displacement of the absorption edge with the temperature in a-SiO_2 is attributed to the presence of heavy holes with $m_h^*=5m_e$, and the tunneling injection of holes into the oxide is attributed to the presence of light holes with $m_h^*=(0.5\pm0.1)m_e$. The contribution of the heavy holes to the tunneling effect is exponentially small compared with that of the light holes. The experiments on the tunneling of holes in SiO_2 confirm the idea that a-SiO_2 contains light holes which correspond to a broad band of bonding Si $3s$, Si $3p$, Si $3d$, O $2p$, and O $2s$ states.

The picture of the transport of holes along the valence band of the oxide is complex and intricate. It is believed that the mobility of holes in SiO_2 (at 300 K) is many orders ($\sim10^{-9}$ cm^2/V·s) lower than the mobility of electrons. The mobility undergoes a strong exponential increase as the temperature rises. There is a great difference between the values of the activation energy for hole transport in a-SiO_2 given by different investigators. According to the data obtained by Hughes,[54] the activation energy for hole transport equals 0.16 eV in the 300–500 K range. This energy is associated with the motion of a polaron along O $2p_\pi$ orbitals. In fields equal to 6×10^5 to 5.5×10^6 V/cm the mobility is not dependent on the field. In another study[55] Hughes obtained the dependence of the mobility on the temperature at 300 K in the form

$$\mu=20\exp\left(\frac{-0.6\text{eV}}{kT}\right)\frac{\text{cm}^2}{\text{V}\cdot\text{s}}. \quad (7)$$

McLean *et al.*[56] observed a strong exponential dependence of the mobility of holes on the electric field and an activation energy equal to 0.39 eV. Thus, the experimental results on hole transport obtained by different investigators are not reproduced. An analysis of the experimental data led Curtis *et al.*[57] to the conclusion that the electrons and holes in the oxide on silicon have comparable (high) mobilities.

The theories on the low mobility of holes in a-SiO_2, which is caused by their polaron mechanism of transport along the O $2p_\pi$ orbitals, have become widely accepted.[26,54] These theories are used, in particular, to account for the buildup of a positive charge in the oxide on silicon during radiation treatments (the generation of electron–hole pairs).[58]

The following arguments can be brought against the polaron mechanism of hole transport along the O $2p_\pi$ orbitals.

1) The parameters characterizing polaron transport along the O $2p_\pi$ orbitals are determined by fundamental properties of SiO_2[the values of ε, ε_∞, the O–O distances (2.65 Å), etc.]. These parameters should not depend on the technology in a first approximation. A strong dependence of the hole mobility on the technology used to prepare the oxide is observed experimentally.

2) In the case of the localization of holes in the O $2p_\pi$ orbitals, the buildup of a positive charge under the action of radiation should occur in the bulk of SiO_2 and should not depend on the technology in a first approximation. The experimental results provide evidence that the buildup of the positive charge occurs in a thin layer with a thickness of ~100 Å near the Si–SiO_2 boundary.[59] Defects, i.e., oxygen vacancies in the form of ≡Si–Si≡ bonds, serve as the capture centers.[60]

3) From the standpoint of the electronic structure of SiO_2, it can be argued that along with the hopping along the weakly overlapping O $2p_\pi$ orbitals, motion is possible along the bonding Si $3s$, Si $3p$, Si $3d$, O $2p$, and O $2s$ orbitals. In the latter case hole transport corresponds to a small effective mass and greater overlapping of the wave functions of the Si and O atoms. The motion of holes along the closely arranged Si and O atoms (1.63 Å) seems preferable to hopping along distantly spaced O atoms (2.65 Å).

It seems that the "intrinsic" mobility of the holes in SiO_2 is determined by the same mechanisms as in the case of electrons. The strong exponential dependence of the hole mobility on the temperature seems to be caused by the presence of hole traps (defects) in the oxide. The energy of the traps in the oxide depends on the technology used to prepare the oxide. Such ideas account for the nonreproducibility of the mobility data and the values of the positive charge obtained by different investigators.

It is perfectly likely that the "intrinsic" mobility of holes in SiO_2 has a value of 20 cm^2/V·s, which appears in the pre-exponential factor in (7). To prove this assertion, it would be interesting to determine the value of the pre-exponential factor on samples having different values of the activation energy for hole transport.

8. CONCLUSIONS

1. The electronic structure of the amorphous oxide on silicon was studied by x-ray emission and photoelectron spectroscopy. The electronic structure of an $Si_8O_{25}H_{18}$ cluster was calculated by the semiempirical MINDO/3 method. The disordering of amorphous SiO_2 was simulated by varying the dihedral Si–O–Si angle and the Si–O bond length. The fluctuations of the angles cause displacement of the E_v and E_c edges of the allowed bands and variation of the width of the band gap.

2. The experiment and the calculations performed indicate that in the upper valence band of SiO_2 there is no gap separating the lower bonding subband from the other two subbands, which are formed mainly from O $2p$ atomic orbitals. The existence of such a gap is predicted by the existing band calculations.

3. The experimental results and the calculations provide evidence that near the top of the valence band there are not only nonbonding O $2p_\pi$ states, which correspond to heavy holes ($m_h^* \simeq 5m_e$), but also bonding Si $3s$, Si $3p$, Si $3d$, O $2p$, and O $2s$ states. The latter correspond to light holes with an effective mass $m_h \simeq 0.5m_e - 1.3m_e$.

4. The theories regarding the localization and transport of holes in amorphous SiO_2 were revised in view of the special features of the electronic structure. According to these theories, holes are transported in SiO_2 by transitions along Si–O–Si bonds, rather than by hopping between the nonbonding O $2p_\pi$ orbitals.

We thank Yu. P. Kostikov for helping to perform the measurements of the photoelectron spectra and Yu. N. Romashchenko for helping to perform the measurements of the emission and quantum-efficiency spectra.

[1] A. R. Silin' and A. N. Trukhin, *Point Defects and Elementary Excitation in Crystalline and Glassy SiO_2* [in Russian], Zinatne, Riga, 1984.
[2] V. A. Gritsenko, *Structure and Electronic Structure of Amorphous Insulators in Silicon MIS Structures* [in Russian], Nauka, Novosibirsk, 1994. W. Y. Ching, Phys. Rev. B **26**, 6622 (1982).
[3] R. P. Gupta, Phys. Rev. B **32**, 8278 (1985).
[4] A. H. Edwards and W. B. Fowler, J. Phys. Chem. Solids **46**, 841 (1985).
[5] V. O. Sokolov and V. B. Sulimov, Phys. Stat. Sol.(b) **135**, 369 (1986).
[6] E. A. Repnikova, L. A. Aleshina, V. A. Gurtov, and A. D. Fofanov, Poverkhnost' Fiz. Khim. Mekh. **4**, 65 (1989).
[7] I. A. Britov, V. A. Gritsenko, and Yu. N. Romashchenko, Zh. Éksp. Teor. Fiz. **89**, 562 (1985) [Sov. Phys. JETP **62**, 321 (1985)].
[8] I. A. Brytov and Yu. N. Romashchenko, Fiz. Tverd. Tela (Leningrad) **20**, 664 (1978) [Sov. Phys. Solid State **20**, 384 (1978)].
[9] G. Hollinger, Y. Jugnet, and T. M. Due, Solid State Commun. **22**, 277 (1977).
[10] R. J. Powell and M. Morad, J. Appl. Phys. **49**, 2499 (1978).
[11] A. M. Goodman, Phys. Rev. **152**, 780 (1966).
[12] Y. Xu and W. Y. Ching, Phys. Rev. B **44**, 1148 (1991).
[13] D. L. Grisco.n, J. Non-Cryst. Solids **24**, 155 (1977).
[14] R. C. Bingham, M. J. S. Dewar, and D. H. Lo, J. Am. Chem. Soc. **97**, 1285 (1975).
[15] G. M. Bartenev, S. M. Brekhovskikh, A. Z. Varisov *et al.*, Izv. Akad. Nauk SSSR, Neorg. Mater. **6**, 1553 (1970).
[16] S. T. Pantelides and W. A. Harrison, Phys. Rev. B **13**, 2667 (1976).
[17] R. N. Nucho and A. Madhukar, Phys. Rev. B **21**, 1576 (1980).
[18] A. O. Litinskiĭ and A. S. Zyubin, Zh. Strukt. Khim. **25**, 11 (1984)[J. Struct. Chem. USSR **25**, 516 (1984)].
[19] R. Tohmon, Y. Shimogaichi, H. Mizuno *et al.*, Phys. Lett. **62**, 1388 (1989).
[20] F. J. Feigl, W. B. Fowler, and K. L. Yip, Solid State Commun. **14**, 225 (1974).
[21] D. L. Griscom, E. J. Friebele, and G. H. Sigel, Solid State Commun. **15**, 479 (1974).
[22] R. A. Devine and J. Arndt, Phys. Rev. B **35**, 9376 (1987).
[23] J. R. Chelikowsky and M. Schulter, Phys. Rev. B **15**, 4020 (1977).
[24] T. H. Di Stefano and D. E. Eastman, Phys. Rev. Lett. **27**, 1560 (1971).
[25] N. F. Mott, Adv. Phys. **26**, 363 (1977).
[26] D. Lohez and M. Lannoo, Phys. Rev. B **27**, 5007 (1983).
[27] A. G. Bennett and L. M. Roth, Phys. Chem. Solids **32**, 1251 (1971).
[28] A. Simunek and G. Wiech, J. Non-Cryst. Solids **137/138**, 903 (1991).
[29] E. P. Domashevskaya, Yu. K. Timoshenko, V. A. Terekhov *et al.*, J. Non-Cryst. Solids **114**, 495 (1989).
[30] R. C. Hughes, Phys. Rev. Lett. **30**, 1333 (1973).
[31] A. M. Goodman, Phys. Rev. **164**, 1145 (1967).
[32] R. C. Hughes, Phys. Rev. Lett. **35**, 449 (1975).
[33] C. N. Berglund and R. J. Powell, J. Appl. Phys. **42**, 573 (1971).
[34] D. R. Young, J. Appl. Phys. **47**, 2098 (1976).
[35] K. Reimann and D. Onnasch, Z. Phys. B **23**, 239 (1976).
[36] K. K. Thornber and R. D. Feynman, Phys. Rev. B **1**, 4099 (1970).
[37] H. J. Fitting and J. U. Friemann, Phys. Status Solidi A **69**, 349 (1982).
[38] M. V. Fischetti, D. J. Di Maria, S. D. Brorson, *et al.*, Phys. Rev. B **31**, 8124 (1985).
[39] M. Lenzlinger and E. H. Snow, J. Appl. Phys. **40**, 278 (1969).
[40] Z. A. Weinberg, W. C. Johnson, and M. A. Lampert, J. Appl. Phys. **47**, 248 (1976).
[41] G. Krieger and R. M. Swanson, J. Appl. Phys. **52**, 5710 (1981).
[42] Z. A. Weinberg and A. Hartstein, Solid State Commun. **20**, 179 (1976).
[43] A. P. Kovchavtsev, Fiz. Tverd. Tela (Leningrad) **21**, 3055 (1979) [Sov. Phys. Solid State **21**, 1758 (1979)].
[44] J. Maserjian, J. Vac. Sci. Technol. **11**, 996 (1974).
[45] J. Maserjian and N. Zamani, J. Appl. Phys. **53**, 559 (1982).
[46] M. V. Fischetti, D. J. Di Maria, L. Dori *et al.*, Phys. Rev. B **35**, 4404 (1987).
[47] V. M. Efimov, E. E. Meerson, and A. A. Evtukh, Phys. Status Solidi A **91**, 693 (1985).
[48] V. A. Gurtov, O. N. Ivashchenkov, and V. V. Pogulyaev, Mikroelektronika **16**, 470 (1987).
[49] J. G. Simmons, F. L. Hsueh, and L. Faraone, Solid-State Electron. **27**, 1131 (1984).
[50] V. A. Gritsenko and E. E. Meerson, Mikroelektronika **17**, 349 (1988).
[51] I. A. Brytov, V. A. Gritsenko, Yu. P. Kostikov *et al.*, Fiz. Tverd. Tela (Leningrad) **26**, 1685 (1984) [Sov. Phys. Solid State **26**, 1022 (1984)].
[52] I. T. Goldmanis, *Electronic Processes and Structure of Defects in Glassy Systems* [in Russian], Izd. Latv. Gos. Un-ta, Univ. Riga, 1982, p. 154.
[53] R. C. Hughes, Phys. Rev. B **15**, 2012 (1977).
[54] R. C. Hughes, Appl. Phys. Lett. **26**, 436 (1975).
[55] F. B. McLean, H. E. Boesch, and J. M. McGarry, Jr., IEEE Trans. Nucl. Sci. **NS-23**, 1506 (1976).
[56] O. L. Curtis, Jr., J. R. Srour, and K. Y. Chiu, J. Appl. Phys. **45**, 4506 (1974).
[57] V. A. Gurtov, A. I. Nazarov, and I. V. Travkov, Fiz. Tekh. Poluprovodn. **24**, 969 (1990) [Sov. Phys. Semicond. **24**, 611 (1990)].
[58] S. T. Chang and S. A. Lyon, Appl. Phys. Lett. **48**, 136 (1986).
[59] H. S. Witham and P. M. Lenahan, Appl. Phys. Lett. **51**, 1007 (1987).

Translated by P. Shelnitz